AD-A159 633 APPLICATION OF DIGITAL INTERFEROGRAM EVALUATION TECHNIQUES(U) ARMY RESEARCH AND TECHNOLOGY LABS MOFFETT FIELD CA AEROMECHANICS LAB F BECKER ET AL. 1985 1/1

UNCLASSIFIED F/G 20/4 NL

END
DATE FILMED
85

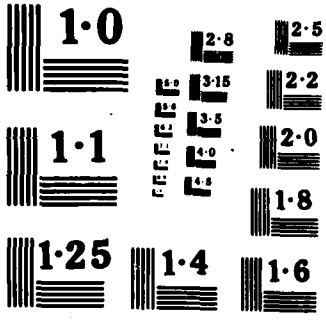
1·0
1·1
1·25
1·4
1·6
1·8
2·0
2·2
2·5
2·8
3·15
3·5
4·0

(1)

AIAA'85

AIAA-85-0037
Application of Digital Interferogram Evaluation Techniques

Friedhelm Becker and Yung H. Yu
Aeromechanics Laboratory
U.S. Army Research and Technology Laboratories-AVSCOM
Moffett Field, CA

AIAA 23rd Aerospace Sciences Meeting
January 14-17, 1985/Reno, Nevada

APPLICATION OF DIGITAL INTERFEROGRAM EVALUATION TECHNIQUES TO THE MEASUREMENT OF THREE-DIMENSIONAL FLOW FIELDS

Friedhelm Becker* and Yung H. Yu†
Aeromechanics Laboratory, U.S. Army Research and Technology Laboratories (AVSCOM)
Ames Research Center, Moffett Field, California

Abstract

A system for digitally evaluating interferograms, based on an image-processing system connected to a host computer, has been implemented. The system supports one- and two-dimensional interferogram evaluations. Interferograms are digitized, enhanced, and then segmented. The fringe coordinates are extracted, and the fringes are represented as polygonal data structures. Fringe numbering and fringe interpolation modules are implemented. The system supports editing and interactive features, as well as graphic visualization. An application of the system to the evaluation of double-exposure interferograms from the transonic flow field around a helicopter blade and the reconstruction of the three-dimensional flow field is given.

Introduction

Holographic interferometric techniques have been widely used in recent years in the area of aerodynamics for flow visualization and quantitative measurements of flow properties, particularly for large field measurements in two- and three-dimensional transonic flows.[1-4]

Interferometric techniques can be used to measure the optical path-length differences (OPDs) between the actual refractive index field $n(x,y,z)$ and a reference field n_o, in either the undisturbed flow or in the test section without flow. The path-length differences in the plane of observation, measured along the probing rays L in units of the wavelength λ, are registered as phase shifts $\Delta\psi$ of the fringes in an interferogram,

$$OPD = \frac{\Delta\psi\lambda}{2\pi} = \int_L (n - n_o)ds = N\lambda \qquad (1)$$

where N is the fringe-order number. The fringes in an interferogram represent contour lines of equal OPD.

In the two-dimensional case, in which a constant refractive index along the probing rays is assumed, the OPD is directly related to the refractive index, and one interferogram is sufficient to obtain the flow field at any location of interest in the field of view.

In the general case, however, in which the flow field is asymmetric, a set of interferograms has to be recorded at different viewing angles around the field in order to reconstruct the flow field. Such an interferogram is a projection of the index of the refractive index field as it represents line integrals of a scalar variable along rays. In general, the line integral can be written

$$N_\phi(\xi,z) = \frac{1}{\lambda} \int_{L_\phi(\xi,z)} [n(x,y,z) - n_o]ds \qquad (2)$$

where (ξ,z) denote the coordinates in the plane of the interferogram and where $L_\phi(\xi,z)$ is a path length through the object.

The refractive index at any given point in the flow field may be obtained by applying the methods of computer-assisted tomography (CAT) to invert the integral equation (2). In the refractionless limit, which is assumed here, the light rays passing through a horizontal plane (z = const) of the phase object form the fringe-order function along a straight horizontal line in the plane of the interferogram. This assumption, which is valid in the actual case, as shown by a numerical simulation,[5] considerably simplifies the numerical reconstruction procedure, because it makes it possible to reduce the three-dimensional reconstruction problem to a two-dimensional one by processing horizontal planes independently.

One important step between recording the interferograms and applying tomographic reconstruction techniques, however, is the evaluation of the interferograms, that is, reading fringe positions and fringe numbers. Up to now, most interferograms from aerodynamic tests have had to be evaluated by either reading fringe numbers and their positions manually or by tracing the fringe lines by hand with the help of a tracking device (for instance a graphic tablet). Manual evaluation, is a very time-consuming and inaccurate procedure, however, and it is evident that in the current application, where large numbers of interferograms have to be evaluated at several horizontal planes, utilization of an automatic fringe-reading procedure would enhance the evaluation and would make the interferometric technique a much more powerful measurement tool.

Different approaches can be used to automatize the analysis of the interferograms. One is direct phase-measurement interferometry in which phase-shifting or heterodyne techniques are used to obtain a set of phase-shifted interferograms from which a relative phase at any given point in the plane of observation may be calculated.[6-10] In a similar approach, point-by-point electronic phase measurement relying on heterodyne interferometry is used.[11] Both methods have been used for measuring deformations of opaque solid objects in nondestructive testing and for making surface measurements in optical quality-testing. Although phase measurements on a point-by-point basis may be very precise, they are inherently slow and require long acquisition times. On the other

---

*NRC-NASA Ames Research Associate.
†Research Scientist.

hand, the application of phase-shifting techniques requires real-time test environments, simultaneous recording of phase-shifted images, or multiple-reference-beam holography.

By introducing enough tilt into the interferometric system (finite-fringe interferometry) it is possible to restrict the fringe field to a straight-line-type pattern. This may then be evaluated by using either Fourier techniques,[12] or spatial synchronous phase detection.[13] These techniques require high fringe densities and therefore high-resolution detection; processing times are also very long.

Other approaches involve the use of image-processing systems to enable a computer-aided evaluation of the real fringe pattern. These systems usually digitize and digitally enhance the fringe pattern. Some are used to perform one-dimensional fringe analysis in nondestructive testing applications,[14-16] to locate fringe centers[17] or fringe sides,[18-22] or to trace the fringe extrema[23] in two-dimensional analysis implementations. Interactive, computer-based systems allow the implementation of sophisticated algorithms for image enhancement, fringe segmentation, error correction, and fringe numbering, all of which have to be applied to evaluate conventionally observed interferograms. Often, the introduction of sufficient tilt (as was done, for example, in Ref. 19) into the interferometric systems used in fluid mechanics is not feasible, so the fringe patterns are generally of higher complexity.

In this paper, digital interferogram analysis methods, developed previously by one of the authors (F.B.),[20,21] implemented on an image-processing systems, is described in more detail and is applied to the reconstruction of three-dimensional transonic flow fields around a rotor blade.

Experimental Setup and Holographic Recording

The double-exposure holographic interferograms of the flow near a hovering 1/7-scale geometric model UH-1H rotor were recently recorded. The one-blade rotor system — 1.05 m span and 0.075 m chord length with NACA 0012 airfoil sections — was run at a tip Mach number of 0.9 in the anechoic hover chamber at the Aeromechanics Laboratory. A pulsed ruby laser was used to record the double-exposed holograms of the transonic flow field around the blade. The diameter of the object beam was 0.6 m, and the total path length was about 30 m.

The first exposure was recorded with the rotor stationary, and the second exposure was recorded with the blade rotating; this was done by synchronizing the laser pulse with the desired blade position. A more detailed description of the holographic system and the rotor test is given in Ref. 3.

Figure 1 shows a top view of the setup with a few typical interferograms recorded at different azimuthal angles. Interferograms at 40 different views were recorded at 2° intervals. As shown in Fig. 1, interferograms recorded at angles of about 90° have very few or no fringes; this is because the optical rays pass through a very thin portion of the refractive index field. However, interferograms recorded at about 180° contain many fringes, for the optical rays pass through the longest portion of the refractive index field along the blade. Shock waves are present in some of these interferograms. Parts of the fringe pattern are blocked off by the shadow of the rotor system in several interferograms.

Interferogram Evaluation

In order to reconstruct the three-dimensional flow field from these interferograms, using tomographic reconstruction techniques, the fringe number-functions along cross sections of a plane parallel to the rotor disk are required. Data from all the views are needed to reconstruct the index of refraction in a particular plane above the blade. Several planes have to be reconstructed to get a three-dimensional flow-field representation. This procedure requires that each interferogram be represented in a form that allows the fringe-order function to be computed at any desired point.

Interferogram evaluation means to extract lines of equal phase $\Delta\psi$ (equal OPD) from the intensity $I(x,y)$ in the two-dimensional interferogram plane, which may be written as

$$I(x,y) = I_0(x,y) + I_1(x,y)\cos(\Delta\psi) \qquad (3)$$

The term I_0 describes the background illumination and the distortions, and I_1 is a modulation term; both may vary over the field of view. The fringe's maxima and minima, or the fringe's sides, are easily detectable lines of equal phase. Each fringe has to be recognized (segmented) from its surroundings and those pixels that represent the constant-phase line have to be picked up. In the simplest case, in which the fringe field is a sinusoidal pattern without any distortions (uniform background illumination), the segmentation can be done by thresholding (level-clipping), using the mean gray value. This procedure would give the fringe-sides as constant-phase lines.

However, most of the holographic interferograms have a nonuniform background illumination with varying contrast and several other distortions (speckle noise, electronic noise). The fringe segmentation in such instances has to be somewhat more sophisticated to enable a trouble-free postprocessing of the extracted data.

Another difficulty in evaluating interferograms from transonic flows is the large variation in fringe density. In all of the near-spanwise views, the fringes are very narrow above the blade, but are very wide in the rest of the field (see Fig. 1). Also, the fringe frequency may change rather rapidly across the field, especially if a shock is present. In applying tomographic reconstruction techniques it is important that the flow field over the entire field of view be known to a high degree of accuracy. But this requirement conflicts with the restricted resolution of the image-processing system. A resolving power of more than 3,000 pixels across the field of view would have been necessary to evaluate these interferograms. In order to achieve the same resolution with the available system, enlarged parts of

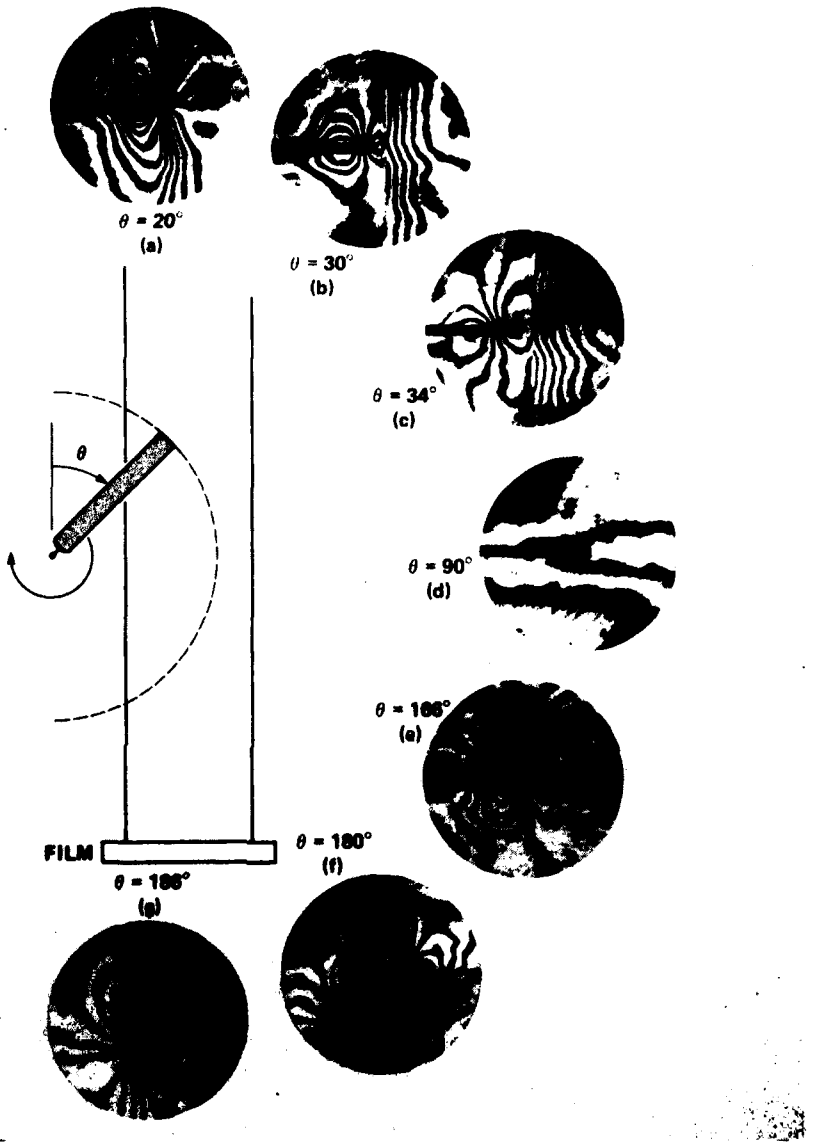

Fig. 1 Top view of the holographic setup and sample interferograms taken at different azimuthal angles.

the interferograms had to be processed individually and had to be merged subsequently.

The evaluation of interferograms using computer-aided methods can be subdivided into the following steps: 1) digitization of the interferograms and image enhancement, 2) fringe segmentation and fringe-coordinate extraction, 3) merging of fringe fields obtained from several magnified views, 4) fringe numbering and correction of fringe disconnections, 5) coordinate transformations, 6) interpolation and extrapolation of fringe-number functions, 7) reconstruction of the flow field, 8) conversion of fringe numbers into refractive index and interesting flow properties.

In the following, a system is described for evaluating interferograms that incorporates all of the evaluation steps mentioned above. All the modules may be called interactively or in batch mode. An editing feature is also implemented, which allows supervision of the evaluation, correction of extraction errors, input of information by hand, modification of fringe numbers, and allows graphic visualization.

Hardware Components

An image-processing system (De Anza IP-6400) connected to a VAX 11/780 host computer provides the main hardware necessary for digitizing the

interferograms and for doing some image-enhancement processing (see Fig. 2).

The resolution of the system is 512 × 512 pixels with an 8-bit intensity range. Currently it is equipped with two of possible four memory planes, as well as with a graphic and an alphanumeric overlay. A frame-grabbing unit can digitize a frame of a video signal in real time (1/30 sec). A black and white video camera (MTI series 68) with resolution (bandwidth) of 18 MHz is connected to this input channel.

The system has an arithmetic-logic unit (ALU), with which real-time addition, subtraction, or comparison of one or more image planes may be made. The contents of each memory plane may be routed through lookup tables before being input to the ALU, to the video-output processor, or to another plane. The actual contents of any image plane or of a combination of image planes is output via a video-output processor and can be shown on a color-display. Each channel has its own color-mapping tables. A joystick control device is used for interactive input. It controls two cursors, which may be used in a number of different operating modes. A color print system (Dunn Instruments model 631) serves as a hardcopy device for the color monitor.

Digitization and Preprocessing

During the recording of the holographic interferograms, two fiducial points were marked in the image plane with a known position relative to the rotor system. This allowed a subsequent coordinate transformation into a space-fixed coordinate system. Each interferogram was then digitized over an area of about 0.18 × 0.25 m^2, and several subsections were enlarged, depending on the fringe density in the interferograms. A scale, aligned to the fiducial marks, was always digitized together with the interferogram so that the position and magnification of the enlarged segments could be identified.

Before segmentation and fringe-coordinate extraction are applied, it may be useful to do some image enhancement to reduce noise. Frame-averaging methods increase the signal-to-noise ratio of the imaging electronic components, thereby improving the picture quality. The averaging is implemented in real time, over 30 frames in 1 sec. Spatial smoothing in a 3 × 3 kernel or in an N × M kernel is useful to reduce high-frequency noise introduced by the holographic procedure (e.g., speckle noise). A histogram equalization may also be done to improve the visibility of a fringe pattern on the display. It has been our experience, however, that this technique must be used with care because it is a nonlinear transformation and tends to amplify noise.

One-Dimensional Evaluation

A one-dimensional interactive processing may be employed, if only one two-dimensional plane of the flow field is reconstructed; hence, only one cross section through each interferogram has to be known. In this case some of the expense required for the full two-dimensional evaluation of the fringe pattern may be avoided. But the procedure has to be interactive, because local information (i.e., knowledge of the fringe locations along one line) is not sufficient to number the fringes correctly or to detect lost fringes or other distortions. In an interactive procedure, information such as acceptance of the segmentation and assigning of fringe numbers has to be given by the user.

Several pattern-segmentation methods that involve gradient operators,[24] adaptive thresholding,[25] Fourier transforms,[15] or piecewise approximation of elementary functions[26,27] have been

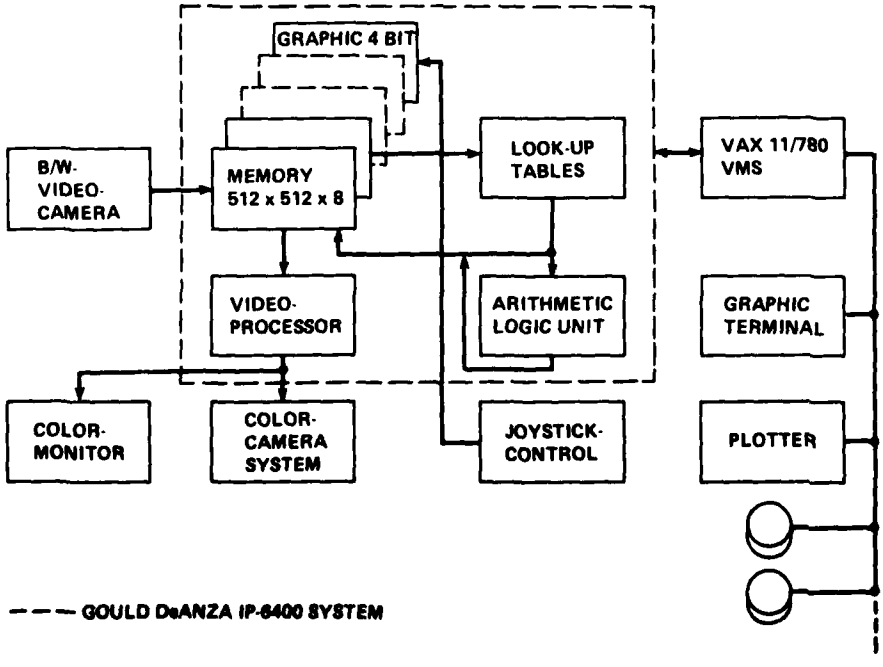

Fig. 2 Image-processing hardware.

reported. The gradient operators, often used in line-detection algorithms, are easy to implement, but they do not work well on sinusoidal patterns, and they are also very noise-sensitive. Adaptive thresholding methods are often used for document scanning and character recognition. They too fail on sinusoidal images. Fourier transform methods are difficult to adapt to fringe fields with varying fringe frequencies across the scan line. Also, they require a certain number of fringes in the cross section and are mainly used for detecting phase shifts in patterns of parallel and equidistant fringes. The piecewise approximation of sinusoidal functions or polynomials has been used in a number of cases in which precise phase measurements had to be made in the presence of speckle noise with only a few fringes in the cross section. These methods generally require excessive computing time, and the convergence and stability depends on a priori estimates of the fringe positions.

A two-pass floating threshold method has been used here for segmentation.[20] In the first pass, the scan line is searched for extrema, using a hysteresis detection scheme. A local extremum is accepted only if it has a minimum gray value difference relative to the last accepted extremum of a different type (after a minimum is accepted, it is searched for a maximum, and vice versa). With the minimum gray value difference, a noise-rejection threshold is established. With the extrema thus found, a step-like threshold function is defined, which settles at the mean gray value between adjacent extrema. Comparison of this function with the original scan line then yields a binary fringe pattern. The transitions from black to white and from white to black define the positions of the left and right fringe sides (see Fig. 3a). This method is fast and quite robust and works well even on fringe fields with abrupt changes in image brightness, fringe density, and contrast. The value of the acceptance threshold is not critical and may usually be varied over a wide range without affecting the segmentation. Also the recognized fringe positions do not depend on the actual value of the acceptance threshold. In images with a known modulation variation, a spatially dependent acceptance threshold may be used.[20]

An example of the segmentation applied to a typical interferogram is shown in Fig. 3b. The actual intensity of a part of a typical scan line is plotted as a solid line and the extracted fringe-positions (left and right sides) are shown as dotted lines.

A program featuring the one-dimensional evaluation digitizes and preprocesses an interferogram and does a fringe-segmentation along a line or along a set of lines through the field of view. The result of the segmentation procedure (a binary fringe pattern) is written back to the image screen for monitoring reasons (see Figs. 3c and 3d). The user may interactively change the acceptance threshold or edit the segmented cross section in heavily distorted regions before he continues to the numbering section. The cursor can be moved to each part of the segmented line, and fringe numbers may be assigned interactively by various commands. The task of assigning fringe numbers is supported by color coding the black parts of the fringes; this shows whether the fringe-order function increases or decreases by 1, or if a discontinuity is present between adjacent fringes. The resulting fringe-order function may also be plotted onto a graphic terminal.

A postprocessing program merges all the data taken from different enlarged portions of an interferogram (as shown in Figs. 3c and 3d) and uses a spline-approximation to interpolate between the fringes. The left- and right-side coordinates, or the middle of the white or black parts of the fringes, may be taken as nodes for the spline approximation. To allow discontinuities in the fringe-order function, a rational spline approximation is used. The type of approximation here may be changed gradually from first-order to third-order polynomials using a parameter derived from the slope of the OPD function (see Fig. 3e).

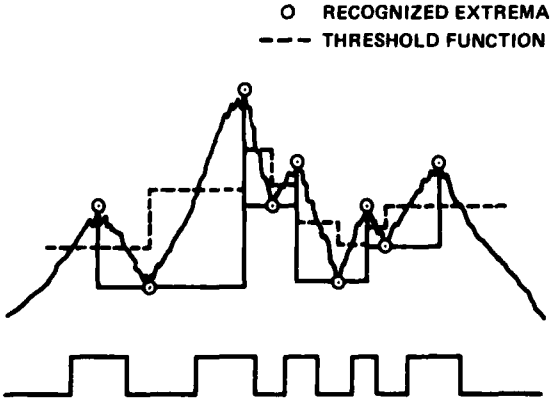

a) Floating threshold fringe segmentation.

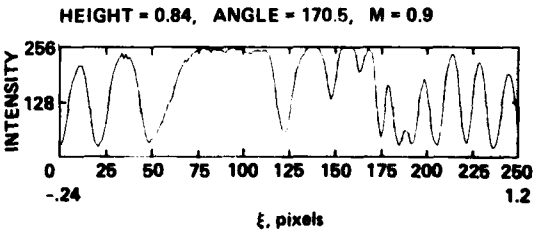

b) Demonstration of the floating threshold fringe-segmentation on a scan line of an actual interferogram.

Fig. 3 Example of one-dimensional processing.

c) Digitized interferogram (182.5) with segmented cross sections superimposed.

d) Evaluation of an enlarged section of the interferogram shown in Fig. 3c.

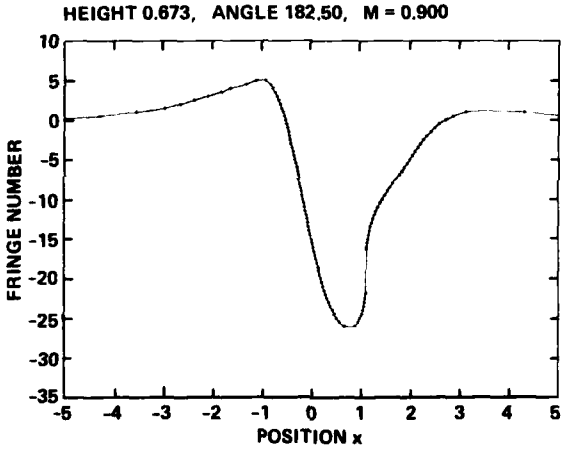

e) Fringe-order function along cross section 3 of interferogram 182.5 after combination of several enlarged subsections and rational spline interpolation.

Fig. 3 Concluded.

Two-Dimensional Interactive Processing

Often the knowledge of only a cross section across the field of view is not sufficient for interpreting a given flow problem; instead, the fringe patterns have to be evaluated over the whole field of view. To facilitate the two-dimensional interferogram evaluation, additional algorithms have been implemented to segment fringes, to extract each fringe's coordinates (trace the fringe sides), and to represent the whole fringe field as a polygonal data structure. Methods for numbering these line fields and detecting extraction errors have been developed. With a two-dimensional interpolation scheme, fractional fringe-order numbers may then be estimated at any given point in the field of view. The methods for two-dimensional evaluation are discussed in the following paragraphs. Typical execution times of the most frequently used modules are given in Table 1.

Fringe Segmentation. The fringe segmentation in the two-dimensional case could be done using the same one-dimensional floating threshold method as described above in a sequential manner for each of the lines of an image. This generally works well for fringe fields running more or less perpendicular to the scan-line, but it may fail if the fringes have significant components parallel to the scan line and if noise or background modulations are present. An example is shown in Fig. 4,

Table 1 Execution times of some hardware and software modules for evaluating interferograms

Function	CPU time (approx.), sec
Digitization, look-up table operations	1/30
Averaging over N frames	N/30
Convolutions[a] (k = kernel elements)	K/30
Binary operations (smoothing, shrinking, expanding)	K/30
Subtraction of approximated background	16
Application of floating threshold method	14
Extraction of fringe coordinates[b]	30
Merging of line fields[b]	10
Numbering, error correction[b]	10
Interpolation[b] (computation of coefficients per polynomial)	0.05

[a]For image processor equipped with three memory pages.
[b]Times depend on the complexity of the image and the number of fringes. The times given are for a typical example, such as that shown in Fig. 5.

where the floating threshold method with fixed acceptance threshold has been applied to a digitized fringe field of low quality (Fig. 4a). The resulting binary patterns are shown after the technique was applied to the scan lines (Fig. 4b) and to columns (Fig. 4c).

In a two-dimensional technique, the nonuniform background would be subtracted and a thresholding with the mean gray value could then be applied. In the case of dual-reference-beam holography, the background correction can be done by subtracting a 180° phase-shifted interferogram.[14] In our case, the approximate background has to be derived from the fringe field itself by a process called "very low-pass" filtering. This technique was also used in Ref. 17, where each pixel was replaced by the mean gray value in a relatively large window. To save computing time, the image area is divided into meshes of suitable size (e.g., 64 × 64 pixels) and the mean gray values are estimated in these meshes. A surface approximation is then constructed by bilinear interpolation between the gray values in every four adjacent mesh points. The discontinuities at the mesh boundaries due to the bilinear interpolation do not affect the segmentation. This surface is then subtracted from the original interferogram, in which an offset of 128 is added to all pixels to avoid negative intensities. An example of the background subtraction is shown in Fig. 4d. A thresholding at level 128 was performed after subtracting the approximated background illumination from the original image in Fig. 4a. The background was constructed on a grid with a mesh size of 64 × 64. The method works better than the floating thresholding in most parts of the image, but does not work as well in the low-contrast areas in the lower middle of the interferogram and in the region of the shock. In the interactive mode, all the above-mentioned methods may be combined so

a) Enlarged digitized subsection of interferogram (184.5) with superimposed grid of meshes of size 64 × 64.

b) Floating threshold method applied to scan lines of Fig. 4a.

Fig. 4 Example of fringe segmentation, binarization.

c) Floating threshold method applied to columns of Fig. 4a.

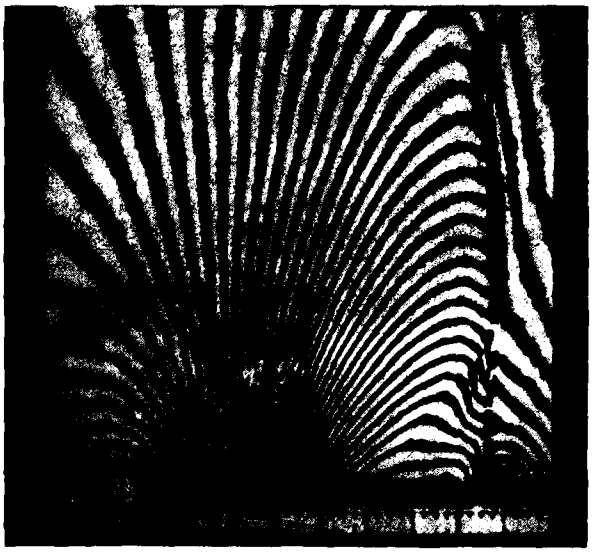

d) Thresholding after background subtraction, computed on the grid in Fig. 4a.

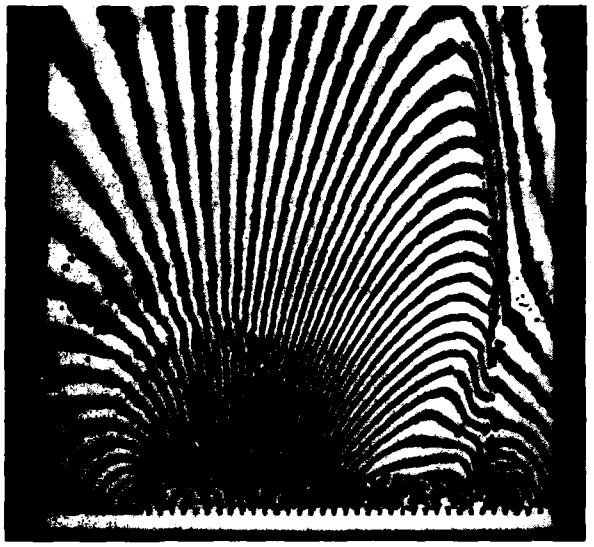

e) Combination of methods b, c, and d.

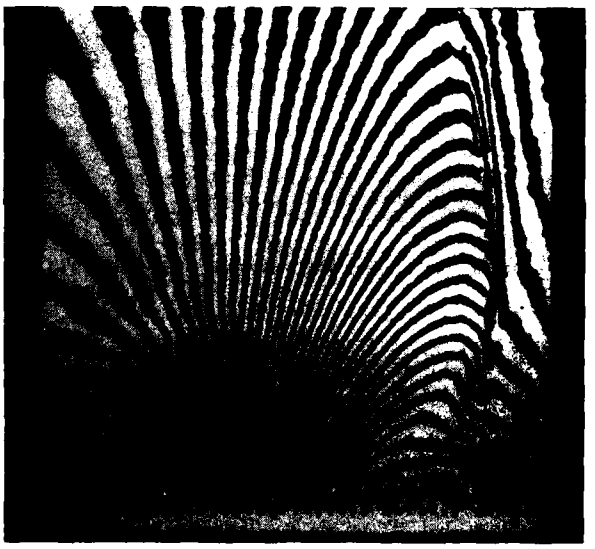

f) Result after binary smoothing and shrinking-expanding operations applied to Fig. 4e.

Fig. 4 Concluded.

that each one works on the whole picture or in selected areas only and it is possible to use the best-suited method for each part of the image. Figure 4e shows the resulting binary pattern after combining background subtraction with horizontal and vertical floating thresholding. After binarization, binary smoothing or shrinking-expanding operations can be applied to reduce pepper and salt noise and to fill in broken lines or to truncate line artifacts (Fig. 4f).

After applying the segmentation procedures, the fringe field is transformed into a binary tone pattern. In some applications, the binary fringe patterns are reduced to line representations using skeletonization techniques,[17-19] giving the middle of the black (or white) fringes as the fringe positions. In our implementation, the coordinates of the fringes are determined at the transition from white to black (and vice versa), giving the fringe sides as the equal phase lines. A sequential tracking procedure similar to a technique used in Ref. 28 is used to trace the fringe positions line by line from the top to the bottom of the picture in order to represent the fringe field as a polygonal data structure.

To reduce the amount of data that must be stored, a redundancy reduction algorithm is activated whenever the temporary storage buffer of

a certain polygon is filled.[29] In this way, the actual polygon is approximated by a subset of vertices of the original polygon within a certain given tolerance range.

If a fringe goes outside the field of view or if a background object such as an airfoil resides inside the fringe field, the visible part of the fringe pattern can be handled by using the points on the boundary as edges of the fringes. Of course, the corresponding polygons may not be connected along the boundary of the background object because they may have different fringe orders. In order to establish the boundary test in a quick, easy, and robust manner, it is not desirable to derive the boundary information from the fringe field itself. Therefore, the geometry of the test region (i.e., the coordinates of the boundary) is used to generate a binary-valued mask which is compared pixel by pixel with the actual interferogram. The boundary of the test section may consist of a number of lines, and there may be several foreground areas or background areas embedded in the field of view. The actual boundary may be generated from the known geometry of the setup or it may be manually entered and interactively drawn onto the screen.

Figure 5 shows an example of a typical fringe-coordinate extraction. An interferogram (Fig. 5a) is digitized over the whole field of view with low resolution. The white lines overlaying the display represent the extracted fringe sides, and the black line represents the border polygon. The border polygon was input by hand before the coordinate extraction in order to mask off background objects and the part of the fringe field with high fringe density. (In our implementation, all the graphics is in color and therefore easier to distinguish from the displayed image.)

The coordinates for each fringe polygon are stored in such an order that the black part of the fringe is always to the right of the polygon. This has some advantages when erroneous parts of the fringe field have to be corrected or when fringe fields have to be combined. Lines may never be connected in a way that a "left" fringe side connects to a "right" one or vice versa, and each line has to have a neighbor of a different type.

The proposed segmentation with subsequent extraction of fringe sides has some advantages over tracking methods that follow the intensity minima or maxima along the fringes.[23] First, the segmentation is more accurate because the fringe sides are better defined due to the maximal slope at the fringe sides. Second, the method works well independently of the fringe density and the fringe contrast. Tracking methods tend to lose orientation in wide fringe areas and are unpredictable if the contrast is varying because they tend to run in the direction of maximal or minimal intensities. Third, all points of the field of view have to be marked in order to avoid multiple tracking of the same fringe and to find all of the fringes. In the fringe side-detection method, two lines per fringe are read in one step; as a result, the accuracy is further increased over that of tracking methods. And fourth, the resulting line structures are simpler because no line branchings occur. For this application, tracking methods are much more unpredictable and slower, and too much intervening action would be necessary to use them successfully.

As was discussed before, it may be necessary to digitize enlarged subsections to resolve regions with high fringe densities. The resulting fringe polygonal field is then combined out of all the individual digitized and processed subsections, starting with the one with highest resolution. To handle the problem of partly overlapping polygonal line fields, a boundary polygon is maintained for each subsection. This defines the definition area for each fringe polygonal field. Upon combination of two overlapping fields, the border polygon of the one with higher resolution (priority) is used to intersect the lines of the other field. Both line fields are then connected at those intersection points. The new border polygon is the border of the combined areas.

Figure 5b shows an enlarged digitized part of the interferogram shown in Fig. 5a, with the extracted fringe polygons overlaying. Figure 5c shows a plot of the resulting polygonal field which was combined from the lines in Figs. 5a and 5b; and two other enlarged sections which are not shown.

Numbering and Error Correction. If distortions are present in the interferogram, for instance, due to diffraction patterns, or if there is insufficient contrast, or if the fringe spacing exceeds the system resolution, as it does in shock or boundary regions, then disconnected fringes may occur and polygonal segments representing fringes of different order may be connected. An example is given in Fig. 6, which is the extracted line field from Fig. 4f. In the lower middle portion of the interferogram in Fig. 6, there is a distortion of the fringe field because of a diffraction pattern, and in the lower right portion the lines are not resolved in the shock region.

In general, local information obtained from the near surroundings of these areas is insufficient to solve the problems; instead, global knowledge about the entire fringe field is necessary. A complete correction of all the incorrectly linked polygonal segments may be performed only during the fringe numbering. However, an error-correcting scheme may be applied before starting the numbering procedure. It uses the geometric parameters of the lines to detect suspicious lines. These are the shape features, for example, circularity (enclosed area divided by the perimeter squared), the distance of the polygonal end points, and the angles between polygonal segments.

A fringe numbering scheme has to introduce the known numbering criteria into an algorithm. They are 1) the fringe-number difference of neighboring fringes must be 0 or 1, 2) fringes of different order do not intersect or touch each other, 3) fringes do not end inside the field of view unless they are circular fringes, and 4) the fringe-number differences integrated along a closed line through the interferogram yield always 0. Furthermore, the a priori known properties of the actual object have to be included.

Different schemes have been developed to number various kinds of fringe fields.[20,21] One scheme suitable for the numbering of erroneously

a) Original digitized interferogram (8.5)—extracted fringe polygons are overlayed in white, the border polygon is written in black.

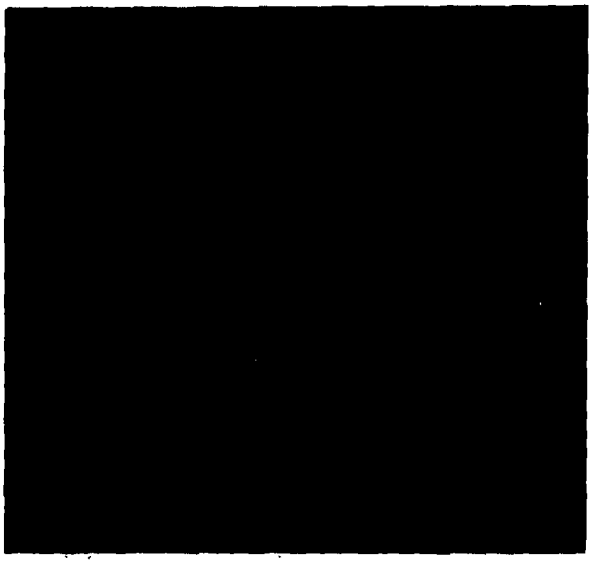

b) Enlarged digitized part of the same interferogram—extracted fringe polygons are overlayed.

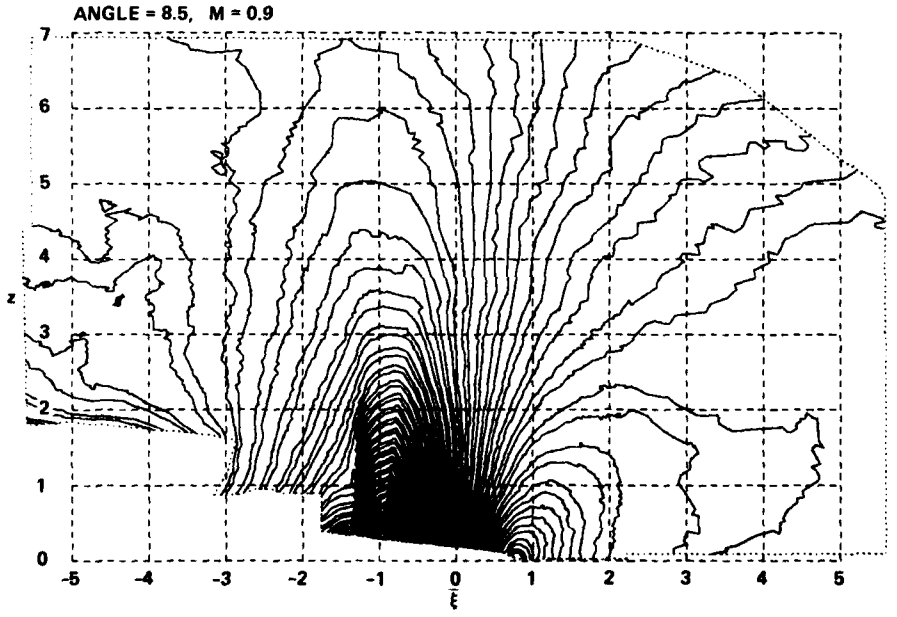

c) Plot of the resulting polygonal field merged from Figs. 6a and 6b and two other enlarged sections not shown.

Fig. 5 Example of fringe polygon extraction and merging of enlarged digitized subsections.

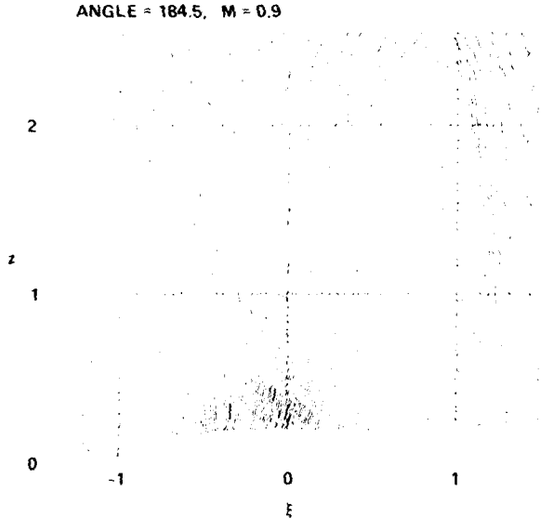

Fig. 6 Extracted line field of Fig. 4f, showing disconnected lines in an area disturbed by a diffraction pattern and in a shock region.

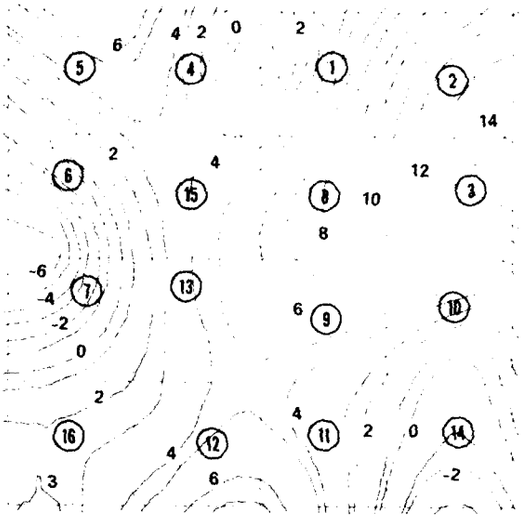

Fig. 7 Fringe numbering. Example of a complex fringe pattern with several minima and maxima; encircled numbers give the order in which the meshes were processed.

extracted line fields shall be described in some detail. The idea of the scheme is based on the fact that in general there are only a few locations that cover a small area, in which the fringe lines are falsely extracted, and that the line field in most parts of the interferogram is represented correctly. The interferogram is divided into rectangular segments by a grid with suitably sized meshes. The line segments inside the meshes are now numbered mesh by mesh, starting at the mesh with the maximal number of line segments and with a minimal number of inversion points of fringe-counting (e.g., a mesh containing parallel lines). The algorithm now looks for the adjacent meshes in which the numbering can continue, that is, those that have at least two consecutive, already numbered line segments at their common grid line. From these meshes, the one showing the best conditions is chosen. If the line numbering of the actual mesh is not in accordance with the numbering of the adjacent meshes, it is put back and handled later. In this way, the meshes containing disconnections are processed after all other meshes have been numbered. The numbering scheme now tries to number the line segments inside the erroneous meshes, using the numbers already known in the neighboring meshes. If a line has to have different numbers, it is cut into two segments at the position where the angle between adjacent polygonal segments is minimal. Another option is to cut at a position where a surface approximation onto the numbered polygonal points exceeds a difference of more than a half order to a point of the actual line to be cut. The procedure assigns relative fringe numbers. The absolute fringe order and direction of increase has to be specified at one location in the field to adjust the other numbers.

As an example of a relatively complex fringe pattern with respect to numbering, Fig. 7 shows the fringe lines of an interferogram of a membrane. The numbering grid is overlayed. The encircled numbers denote the order in which the meshes were processed by the algorithm. Note that the algorithm tends to number parts of the fringe field consisting of similar running lines in a monotonic manner. This is the most basic of the rules used for numbering fringes. It derives from the fact that most physical object functions are monotonic and smooth in most areas of the field of view. If the fringe fields did not fulfil this basic requirement, a fringe numbering without further knowledge of the physical properties of the object would actually be impossible.

Figure 8 shows the numbering grid used for numbering the line field shown in Fig. 6. The

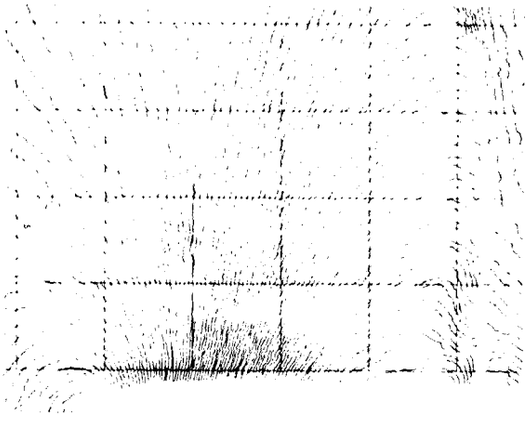

Fig. 8 Numbered and error-corrected line field of Fig. 5c with numbering grid.

meshes containing the shock and the distorted area are detected by the algorithm because of their high number of inversion points. They are numbered after all other meshes have been processed so the lines that could not be numbered uniquely will be cut somewhere in the mesh. The position where this is done, however, may not be the correct one. Often fringes of different order are connected through a shock without any indication of the existence of the shock (see, e.g., Fig. 6). In this case, the area where the shock appears may be masked off by hand editing before starting the numbering (see Fig. 8).

In the edit mode, the fringe polygonal fields may also be numbered manually by drawing a test line into the line field and numbering the intersected fringe lines by several commands using the cursor. Also, all lines may be modified manually in the interactive edit mode before starting the numbering or the postprocessing.

Interpolation. After numbering the fringe lines, the OPD function is defined at a set of contour lines, but most of the mathematical transformations to follow require interpolation of fractional fringe-order numbers. Some methods for interpolating between random points on a surface are discussed in Ref. 30. An algorithm best suited in regard to computation time, as well as in regard to numerical representation, seems to be a local distance-weighted polynomial least-squares approximation. At a given point (a,b) the coefficients of a two-dimensional polynomial of second order

$$P(x,y) = \sum_{k=0}^{2} \sum_{l=0}^{2-k} c_{kl}(x - a)^k (y - b)^l \qquad (4)$$

are estimated to minimize the quadratic form

$$Q = \sum_{r} [P(x_r,y_r) - z_r]^2 w[(x_r - a)^2 + (y_r - b)^2] = \text{Min} \qquad (5)$$

where $w(d^2) = \exp(-kd^2)$ is a weighting function, which gives more weight to the data points (x_r,y_r) having a shorter distance d to the point (a,b) than the more distant points. The additional advantage is that more distant points may be ignored in the computation. The solution of Eq. (5) is performed by solving a system of linear equations (Gauss's method). The parameter k in the weighting function is chosen according to the local data point density. The whole fringe field may be represented with the polygonal coefficients calculated on a regular grid. If a smooth approximation of the OPD surface is desired, a two-dimensional spline function may be defined at the meshes of a rectangular grid using only the zero and first-order coefficients from the previously obtained polynomials.

An advantage of using a polynomial representation is the fact that it is possible to extrapolate the fringe field into regions blocked by background objects. As an example, Fig. 9 shows an interpolated cross section through the numbered polygonal field of Fig. 5c at z = c/3. Note that

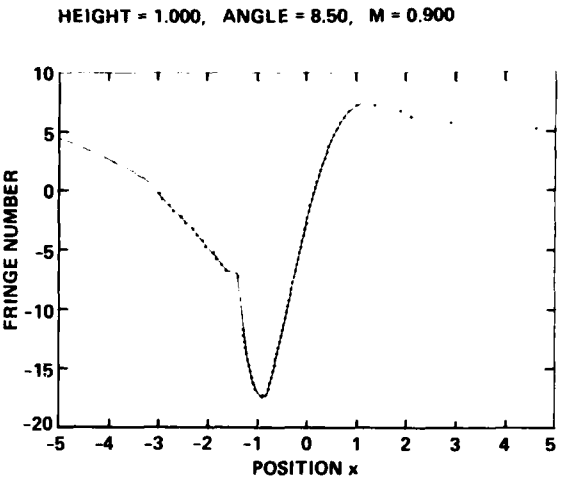

Fig. 9 Interpolated fringe-order function along a cross section at z = c/3 through the numbered line field of Fig. 5c, showing extrapolation to the left. The symbols mark the coordinates of the fringe polygons in the cross section.

the left side of the line is extrapolated over a region of the interferogram blocked off by the rotor system.

Reconstruction

A number of reconstruction algorithms, such as Fourier transform methods, back-projection methods, and iterative methods are covered in the literature (see, for instance, Ref. 31). Here a convolution back-projection algorithm with a filter function proposed in Ref. 32 was chosen, because it generally gives good results, is easy to implement, and is very efficient. The convoluted back-projection is given as

$$g_B(x,y) = \int_0^{\pi} \int_{-\infty}^{\infty} N_\phi(\xi) * F^{-1}\{|r|\} \delta(x \sin\phi + y \cos\phi - \xi) \times d\xi \, d\phi \qquad (6)$$

where $g_B(x,y)$ is the reconstructed field function in a horizontal plane (z = const), and $N_\phi(\xi)$ are the cross sections through the fringe-order functio at angles ϕ to be convolved with the inverse Fourier transform of the abs-function. The integration of the convolved "projections" is done along the lines $L_\phi(\xi)$, which are expressed as

$$\delta(x \sin\phi + y \cos\phi - \xi) \qquad (7)$$

and over all the projections ϕ.

Figure 10a shows a reconstruction of the flow field in a plane 8.28% chord above the blade obtained from the experimental data at 41 views for the angular interval from 8° to 40° and from 140° to 186° in 2° intervals. The missing views are presumed to be zero (those interferograms have only a few or no fringes and were not evaluated). The resolution in the plane is 101 × 101 points,

and 101 rays were used in the projection data at each view (see Fig. 9). The time required for a reconstruction from 41 projections with 101 rays at a grid of 101 × 101 points is about 24 sec of CPU time on a VAX 11/780.

The reconstruction gives a map of the refractive index in the plane. Because the refractive index of gases is proportional to the density ρ (Gladstone-Dale relation),

$$\rho/\rho_o = (n - 1)/(n_o - 1) \tag{8}$$

the density may be directly calculated. Other flow properties, such as pressure, may be obtained by assuming isentropic flow. The perturbation velocity is derived by application of a form of the energy equation to the blade-fixed flow problem

$$v(r) = -\Omega r + \sqrt{(\Omega r)^2 - \frac{2c_o^2}{\gamma - 1}\left[(\rho/\rho_o)^{\gamma-1} - 1\right]} \tag{9}$$

where γ is the specific heat ratio, c_o is the velocity of sound, and Ω is the angular velocity of the blade.

The lines in Fig. 10a are contour lines of the perturbation velocity. This result may be compared with a cross section through a numerically obtained small perturbation potential solution[33] which is shown in Fig. 10b. The basic features of the flow field, the shock position, and the amplitudes are very well confirmed. Differences appear in the velocity profiles across the chord in the tip region of the blade which can be attributed to actual differences in the predicted and measured flow fields. The finite difference code used in the predictions of the flow field does not yet include viscous effects and therefore can not account for the lambda shock effects seen in the measured data.

A more detailed discussion of the reconstruction results and a comparison with hot-wire and pressure measurements is given in Ref. 34.

Conclusions

The features of an image-processor-based system for analyzing interferograms have been described. The system contains algorithms for all steps of digital interferogram processing, from image-processing techniques, such as digitization, enhancement, and segmentation, to graphic data-processing techniques, such as fringe-coordinate extraction, merging of line fields, error correction, fringe numbering, and approximation techniques for interpolating two-dimensional fringe fields. All the modules may be called interactively, and editing features are available to process interferograms even if they are of poor quality. The interactive modes are fully supported by graphic visualization. An application to the reconstruction of a three-dimensional flow field, which was recorded by holographic interferometry at several views around the field, was given. It showed that the digital technique provided better and faster evaluations of the interferograms than could be achieved manually. The full analysis of the flow field under investigation would hardly have been possible had it been necessary to analyze the data manually.

However, in the implementation that was described, some information had to be input

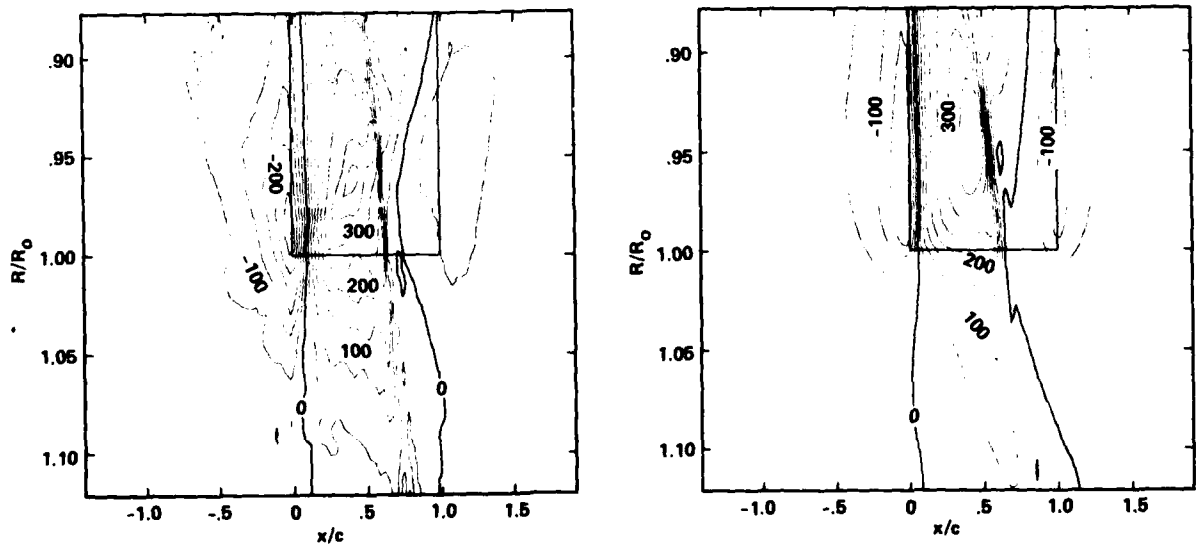

a) Perturbation velocity contours in feet per second as reconstructed from cross sections through 41 interferograms, at 101 × 101 points.

b) Perturbation velocity contours at the same height above the blade as given by a numerical solution of the flow problem.

Fig. 10 Reconstruction of the flow field in a horizontal plane at $z/c = 0.0828$ above the blade. The blade rotates clockwise, the leading edge is at $x/c = 0$ (c is the chord length of the blade, R_o is the blade radius).

manually, even for interferograms of good quality. This included the geometric reference points, the decision whether enlarged subsections should be digitized, the choice of an optimal enlargement factor, the entering of background border polygons, and the reference number for the fringe numbering. In order to use this system in a standard test facility, the interactive action can be further reduced by using the same information for series of interferograms taken under similar conditions.

Acknowledgments

During this work one of the authors (F.B.) was holding an NRC Resident Research Associateship at the NASA Ames Research Center. Part of the interferogram evaluation software was developed previously by one of the authors (F.B.) at the Max-Planck Institut für Strömungsforschung in Göttingen, West Germany. The authors wish to acknowledge the efforts of Mr. John Kittleson of the Aeromechanics Laboratory for providing the quality interferograms used in the tomographic reconstruction process. The enthusiastic support and contribution of Dr. Sanford S. Davis and George Lee at Ames Research Center are gratefully acknowledged. The inspiration and unselfish support of Dr. Fredric H. Schmitz of the Aeromechanics Laboratory made this project possible.

References

[1]Trolinger, J. D., "Laser Instrumentation for Flow Field Diagnostics," AGARDograph 186, 1974.

[2]Johnson, D. A. and Bachalo, W. D., "Transonic Flow About a Two-Dimensional Airfoil—Inviscid and Turbulent Flow Properties," AIAA Paper 78-1117, July 1978.

[3]Kittleson, J. K., "A Holographic Interferometry Technique for Measuring Transonic Flow Near a Rotor Blade," Ninth European Rotorcraft Forum, Paper No. B, Stresa, Italy, Sept. 13-15, 1983.

[4]Lee, G., "Application of Holography to Flow Visualization," NASA TM-84325, Jan. 1984.

[5]Snyder, R. and Hesselink, L., "Optical Tomography for Flow Visualization of the Density Field Around a Revolving Helicopter Rotor Blade," Appl. Opt., Vol. 23, No. 20, 1984, pp. 3650-3656.

[6]Bruning, J. H., Herriott, D. R., Gallagher, J. E., Rosenfeld, D. P., White, A. D., and Brangaccio, D. J., "Digital Wavefront Measuring Interferometer for Testing Optical Surfaces and Lenses," Appl. Opt., Vol. 13, No. 11, 1974, pp. 2693-2703.

[7]Fischer, W. R., Crostack, H.-A., Steffens, H.-D., "Automatische Analyse Holographischer Interferogramme für die zerstörungsfreie Prüfung," Laser 79 Opto-Electronics, Munich 2/6 July 1979, Conf. Proc., IPC Science and Technology Press, London, pp. 404-411.

[8]Yatagai, T. and Kanou, T., "Aspherical Surface Testing with Shearing Interferometer Using Fringe Scanning Detection Method," Opt. Eng., Vol. 23, No. 4, 1984, pp. 357-360.

[9]Smythe, R. and Moore, R., "Instantaneous Phase Measuring Interferometry," Opt. Eng., Vol. 23 No. 4, 1984, pp. 361-364.

[10]ZYGO Phase Measuring Interferometer System, Technical description, Zygo Corp., Middlefield, Ct. 1981.

[11]Dändliker, R., Progress in Optics, Vol. 17, E. Wolf, Ed., North-Holland, Amsterdam, 1980, Ch. 1

[12]Takeda, M., Ina, H., and Kobayashi, S., "Fourier-Transform Method of Fringe-Pattern Analysis for Computer-Based Topography and Interferometry," J. Opt. Soc. Am., Vol. 72, 1982, pp. 156.

[13]Womack, K. H., "Interferometric Phase Measurement Using Spatial Synchronous Detection," Opt. Eng., Vol. 23, No. 4, 1984, pp. 391-395.

[14]Schlüter, M., "Analysis of Holographic Interferograms with a TV Picture System," Optics and Laser Technology, Vol. 12, 1980, pp. 93-95.

[15]Robinson, D. W., "Automatic Fringe Analysis with a Computer Image-Processing System," Appl. Opt., Vol. 22, No. 14, 1983, pp. 2169-2176.

[16]Tichenor, D. A. and Madsen, V. P., "Computer Analysis of Holographic Interferograms for Nondestructive Testing," Opt. Eng., Vol. 18, No. 5, 1979, pp. 469-472.

[17]Nakadate, S., Magome, N., Honda, T., and Tsujiuchi, J., "Hybrid Holographic Interferometer for Measuring Three-Dimensional Deformations," Opt. Eng., Vol. 20, No. 2, 1981, pp. 246-252.

[18]Nakadate, S., Yatagai, T., and Saito, H., "Computer-Aided Speckle Pattern Interferometry," Appl. Opt., Vol. 22, No. 2, 1983, pp. 237-243.

[19]Yatagai, T., Inabu, S., Nakano, H., and Suzuki, M., "Automatic Flatness Tester for Very Large Scale Integrated Circuit Wafers," Opt. Eng., Vol. 23, No. 4, 1984, pp. 401-405.

[20]Becker, F., "Zur automatischen Auswertung von Interferogrammen," Mitteilungen aus dem Max-Planck-Institut für Strömungsforschung, Göttingen, W. Germany, Nr. 74, 1982.

[21]Becker, F., Meier, G. E. A., and Wegner, H., "Automatic Evaluation of Interferograms," Applications of Digital Image Processing IV, Andrew G. Tescher, Ed., Proc. SPIE 359, 1982, pp. 386-393.

[22]Cline, H. E., Holik, A. S., and Lorenson, W. E., "Computer-Aided Surface Reconstruction of Interference Contours," Appl. Opt., Vol. 21, No. 24, 1982, pp. 4481-4488.

[23]Funnel, W. P J., "Image Processing Applied to the Interactive Analysis of Interferometric Fringes," Appl. Opt., Vol. 20, No. 18, 1981, pp. 3245-3250.

[24]Rosenfeld, A. and Kak, A., "Digital Picture Processing," Academic Press, New York, 1976.

[25]To Russel Hsing, "Techniques of Adaptive Threshold Setting for Document Scanning Applications," Opt. Eng., Vol. 23, No. 3, 1984, pp. 288-29

[26]Snyder, J. J., "Algorithm for Fast Digital Analysis of Interference Fringes," Appl. Opt., Vol. 19, 1980, pp. 1223-1225.

[27]Schemm, J. B. and Vest, C. M., "Fringe Pattern Recognition and Interpolation Using Nonlinear Regression Analysis," Appl. Opt., Vol. 22, No. 18, 1983, pp. 2850-2853.

[28]Agrawala, A. K. and Kulkarni, A. V., "A Sequential Approach to the Extraction of Shape Features," Computer Graphics and Image Processing, Vol. 6, 1977, pp. 538-557.

[29]Ramer, U., "An Iterative Procedure for the Polygonal Approximation of Plane Curves," Computer Graphics and Image Processing, Vol. 1, 1972, pp. 244-256.

[30]McLain, D. H., "Drawing Contours from Arbitrary Data Points," Computer J., Vol. 17, No. 4, 1974, pp. 318-324.

[31]Herman, G. T., Ed., "Image Reconstruction from Projections, Implementation and Applications," Topics in Appl. Phys., Vol. 32, Springer, Berlin, 1979.

[32]Shepp, L. A. and Logan, B. F., "The Fourier Reconstruction of a Head Section," IEEE Trans. NS-21, No. 3, 1974, pp. 21-43.

[33]Caradonna, F. X., "The Transonic Flow on a Helicopter Rotor," Ph.D. Dissertation, Stanford Univ., Stanford, Calif., 1978.

[34]Kittleson, J. K. and Yu, Y. H., "Reconstruction of a Three-Dimensional Transonic Rotor Flow Field from Holographic Interferogram Data," Paper No. 85-0370, AIAA 23rd Aerospace Sciences Meeting, Reno, Nev., Jan. 14-17, 1985.


DAT
FILM